Journal of MATERIALS RESEARCH

Article
DOI:10.1557/s43578-023-00931-z

Plasmonic properties of Ag@TiO$_2$ nanostructures improve the graphitization of polyacrylonitrile and the mechanism

Zhengdong Zhang[1,b)], Yaoning Bai[1,b)], Xinru Li[1], Taoyuan Ouyang[1], Yuwei Yan[1], Nan Sun[1], Jianqi Liu[1], Xiaoming Cai[2], Jinming Cai[1], Honglin Tan[1,a)]

[1] *Faculty of Materials Science and Engineering, Kunming University of Science and Technology, Kunming 650000, Yunnan, People's Republic of China*
[2] *Faculty of Mechanical and Electrical Engineering, Kunming University of Science and Technology, Kunming 650000, Yunnan, People's Republic of China*
a) Address all correspondence to this author. e-mail: 852419171@qq.com
b) These authors contributed equally to this work.

Received: 17 September 2022; accepted: 2 February 2023; published online: 24 February 2023

Plasmonic nanostructures can catalyze reactions at near room temperature via surface plasmon resonance (SPR). Herein, we have successfully prepared Ag@TiO$_2$ photocatalysts with the plasmonic properties by applying magnetron sputtering. The results of optical and electrochemical measurements indicated that Ag@TiO$_2$ nanoparticle composite structure can expand the light response area and improve the efficiency of hot electron–hole pair separation. Additional experimental results verify that the SPR effect of silver nanoparticles is an important trigger for the photochemical transformation of Polyacrylonitrile (PAN); and the Ag@TiO$_2$ nanostructures exhibit high catalytic activity for enhancing the catalytic graphitization of PAN in comparison with the bare Ag. The Raman peak I$_D$/I$_G$ ratio of Ag@TiO$_2$-catalyzed PAN at 80 °C is 0.87, which is 17% lower than that of pure Ag-catalyzed PAN. The accuracy of the experimental results was also clearly confirmed by simulating the electromagnetic response of Ag@TiO$_2$ photocatalysts using the finite difference time domain (FDTD) method.

Introduction

Since the beginning of the twenty-first century, with the development of social economy, a series of climate, environmental and energy problems have arisen [1]. Now, people usually use photocatalytic reactions to alleviate the above problems [2]. Among them, surface plasmons can drive catalytically inert molecules under mild conditions, which makes them gradually become a hot spot in the field of photocatalysis [3]. For instance, plasmonic nanostructures can convert CO$_2$ into valuable hydrocarbons at room temperature and atmospheric pressure [4]. In addition, plasmonic nanostructures can also catalytically modify organics to make them more functional [5, 6].

In previous studies, Most PAN-based carbon materials can only be graphitized at high temperature without the use of catalysts [7]. In order to increase the degree of graphitization of polyacrylonitrile carbon materials, a method of adding a catalyst can be used, which is called catalytic graphitization. In recent years, much effort has been devoted to improving the degree of graphitization of carbon. In addition, many studies have reported on the catalytic graphitization of polyacrylonitrile by boron. Boron can replace carbon in the graphite lattice, so that the polyacrylonitrile-based carbon material can be graphitized uniformly [8]. He et al. investigated Synergistic catalytic effect of Ti–B on the graphitization of polyacrylonitrile-based carbon fibers [9]. It has also been reported to load rare earth elements on the surface of carbon materials to explore the performance of catalyzing graphitization [10, 11]. However, this technology often requires consume substantial amounts of energy, the high operational cost. There has been an explosion of interests and activities on plasmon-driven catalytic reactions [12, 13]. Along these lines, the low-temperature catalytic graphitization performance of PAN molecules can be explored by this method.

Plasmonic metals silver (Ag), copper (Cu), and aluminum (Al) are widely used in catalysis because of their surface plasmon resonance (SPR) effect [14]. Ag is not easily oxidized in air and shows excellent chemical stability compared to Cu plasmonic metal. TiO_2-based materials are the most widely studied catalytic materials, which are widely used in the field of environment and energy [15–17]. Moreover, enlarging the response region of light and improving the separation efficiency of hot electron–hole pairs can be achieved by constructing plasmonic metal/semiconductor hybrid structures and heterojunction [18–27]. Therefore, Ag@TiO_2 composite material is effectively prepared by magnetron sputtering method. And this catalyst is used to enhance the catalytic graphitization of PAN. Additionally, this compares favorably with published reports of enhancement of the catalytic graphitization of PAN by incorporating Cu nanostructures as plasmonic photocatalyst [28–30]. What's more, catalytic graphitization of polyacrylonitrile (PAN) using Ag@TiO_2 nanostructures has been rarely investigated in depth.

In this work, to further improve the graphitization of polyacrylonitrile and reduce graphite defects at low temperatures, we have successfully prepared Ag@TiO_2 photocatalysts with the plasmonic properties by applying magnetron sputtering. We have investigated the photochemical conversion of polyacrylonitrile on Ag@TiO_2, Ag, and TiO_2 substrates, respectively. The UV–vis diffuse reflectance absorption spectra, PL experiments, the photocurrent response experiments and EIS experiments revealed the reason why Ag@TiO_2 photocatalysts enhance the graphitization of polyacrylonitrile. Using the physical dimensions determined in the experiments, the Ag@TiO_2 nanostructures were simulated by FDTD to further verify the experimental results.

Results and discussion

Characterization of Ag@TiO_2 composites

Figure 1(a) shows the SPR effect of Ag nanoparticles. The noble metal Ag has gradually developed into a promising light-harvesting material due to its tunable light absorption ability and its surface plasmon resonance (SPR) [31]. Anatase, brookite, and rutile are polymorphs of TiO_2, among which the most widely used polymorph for photocatalysis is anatase [32]. Figure 1(b) shows the crystal structure of anatase TiO_2. Ag@TiO_2 composites were prepared by magnetron sputtering in order to expand the light response region and improve the efficiency of hot electron–hole pair separation in photocatalysis. Figure 1(c) showed the schematic representation for the preparation of Ag@TiO_2.

Ag@TiO_2 composite material is effectively prepared by magnetron sputtering method. First, Ag and TiO_2 were sequentially deposited on the crystalline silicon wafer substrates in magnetron sputtering equipment. After that, the sample was annealed for 1 h under the conditions of an argon atmosphere and 450 °C, the main purpose is to make the silver film grow into fine and uniform grains. As shown in Fig. 2(a), the Ag@TiO_2 nanoparticles are spherical. However, similar results were not obtained when the order of Ag and TiO_2 deposited on the crystalline silicon wafer substrate is changed under the same conditions, as shown in Fig. 2(c), where the nanoparticle structure is irregular. It is well-known that noble metal Ag nanostructures exhibits outstanding plasmonic properties [33]. Besides, metal–semiconductor heterostructures provides a rich variety of localized

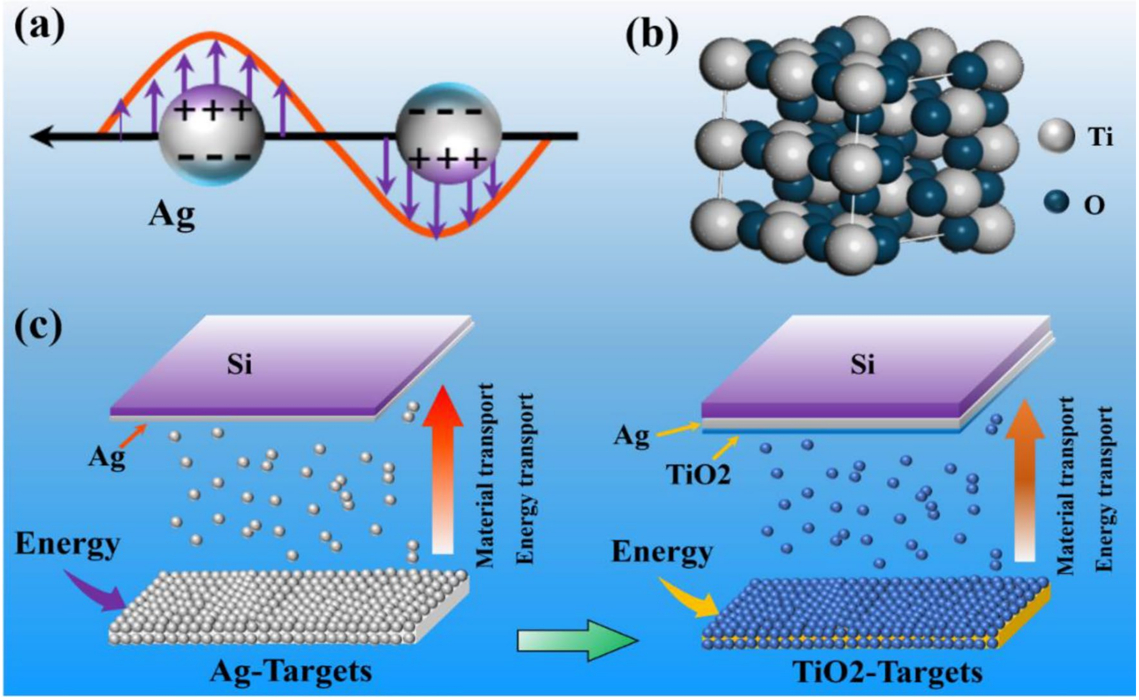

Figure 1: (a) Shows the SPR effect of Ag nanoparticles. (b) Shows the crystal structure of anatase TiO_2. (c) The preparation process of Ag@TiO_2 substrate.

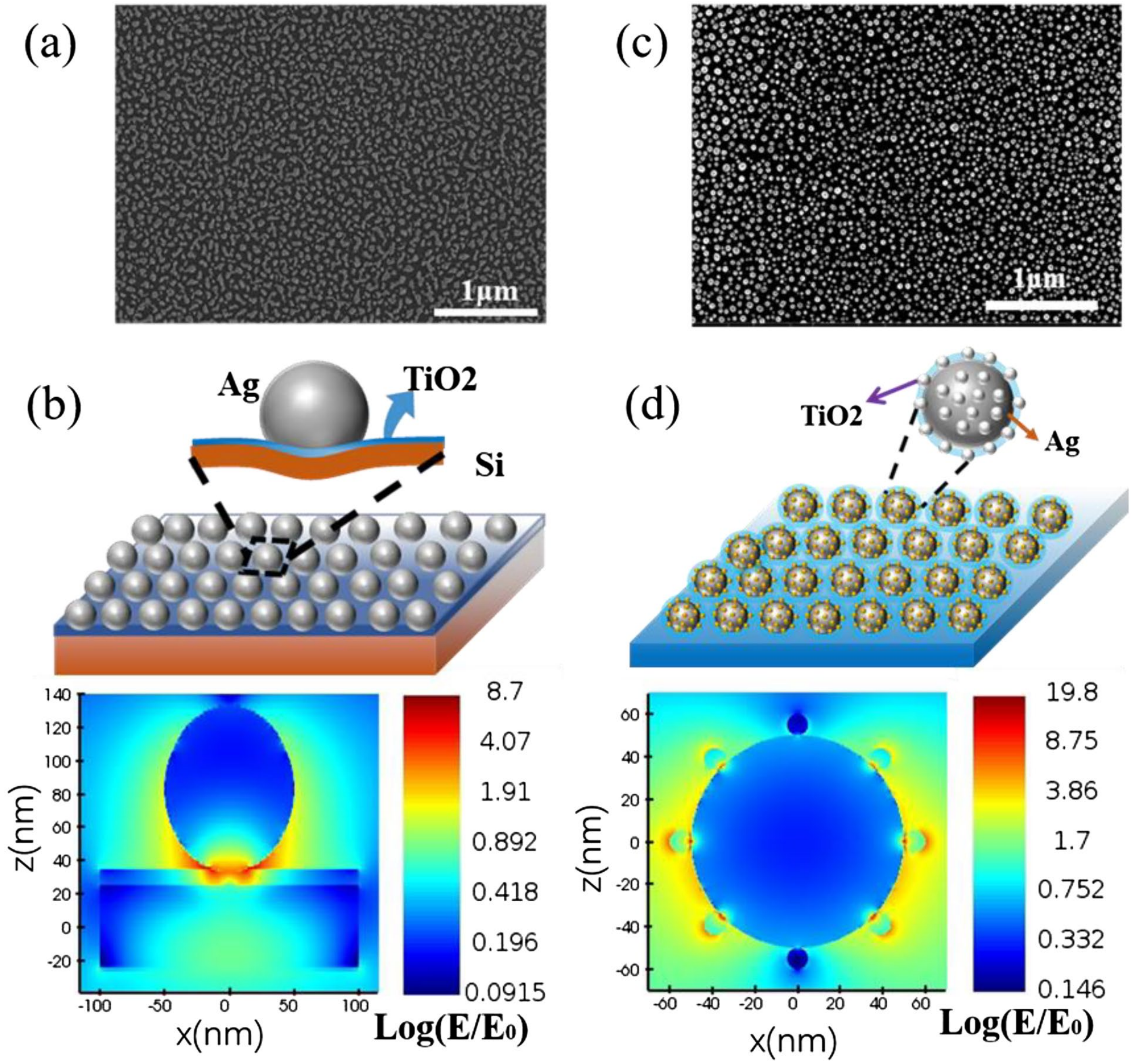

Figure 2: (a) SEM image of the TiO_2/Ag nanostructure; (b) model and local field intensity distribution corresponding to (a); (c) SEM image of the Ag@TiO_2 nanostructure; (d) model and local field intensity distribution corresponding to (c).

surface plasmon resonances [34]. Interestingly, it was found that the SPR facilitated some chemical reactions. To further optimize the experimental process and screen the best plasma photocatalytic substrate to improve the effect, we used the FDTD method to simulate the local surface plasmon resonance effects of substrate materials obtained in two different ways. Figure 2(b, d) are the corresponding simulation results of Fig. 2(a, c), respectively. The results [Fig. 2(b) and (d)] reveal the local electric field values, and the color bar displayed represents the respective electric field enhancement obtained in each case. As we can see from Fig. 2(b, a) strong local electric field is obtained between the contact gaps when TiO_2 nanoparticles are loaded onto the surface of Ag spherical nanoparticles [6]. We can clearly see that the strength of the localized electric field (Log(E/E_0)) up to 19. However, it does not show a better enhanced electric field when Ag nanoparticles are loaded on the surface of the TiO_2 film, as shown in Fig. 2(d). In contrast, the substrate of TiO_2 nanoparticles loaded on Ag nanoparticles can produce high local field strength, which is beneficial for the catalytic applications.

Scanning electron microscope (SEM) was employed to analyze the morphology of the obtained Ag@TiO_2 sample. From Fig. 3(a), a uniform distribution of small nanoparticles was observed on the Si substrate. The high-magnification SEM image [Fig. 3(b)] reveals that the synthesized nanospheres are approximately 100 nm in diameter. EDS elemental mapping measurements were conducted to examine the elemental distribution

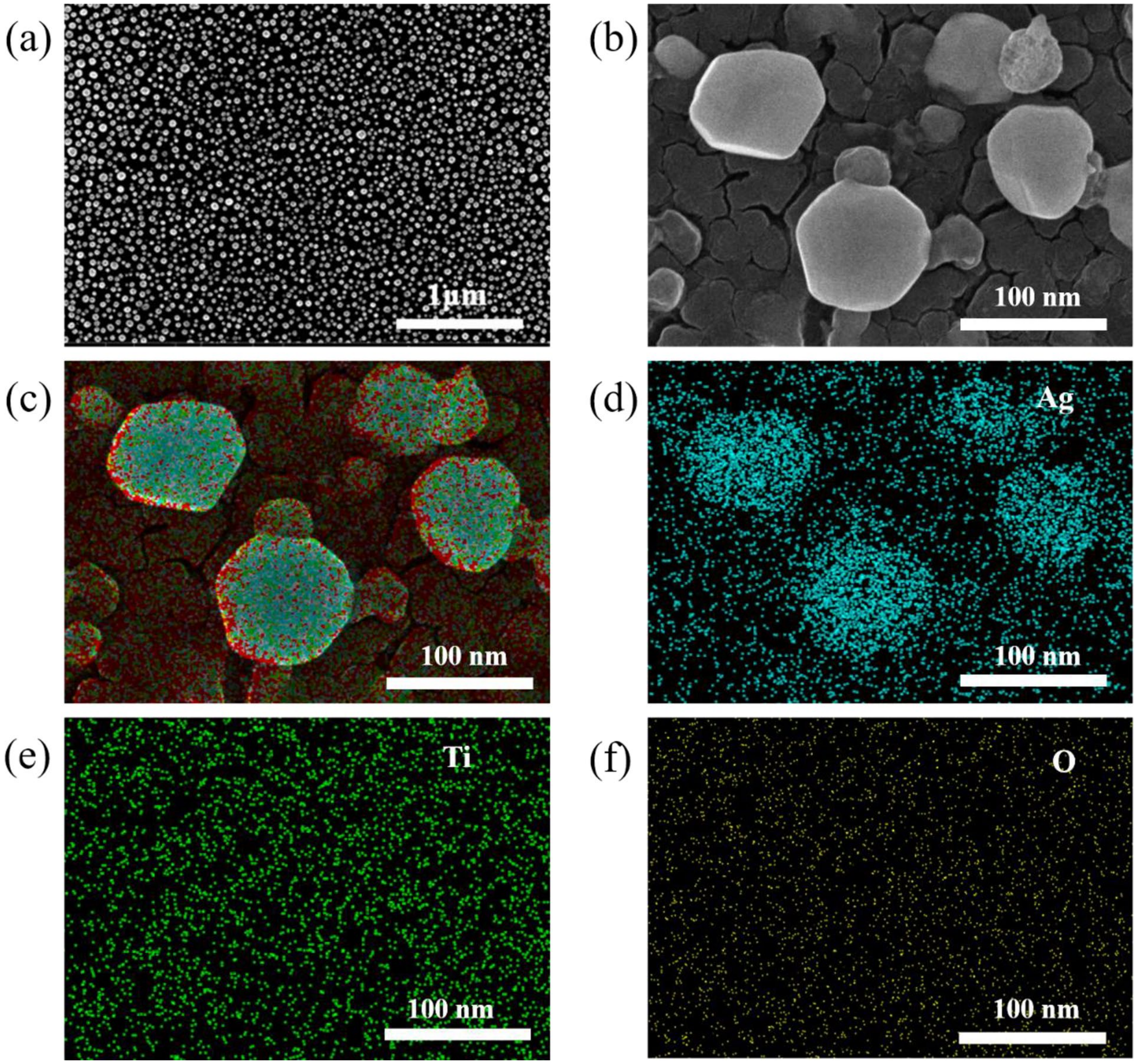

Figure 3: (a) SEM image of Ag@TiO_2. (b) SEM images of CNCs at 50,0000×magnification. (d–f) Energy-dispersive spectrum (EDS) mapping showing the distribution of Ag, Ti and O.

in Ag@TiO_2 [Fig. 3(d–f)]. The mapping measurements show that the distribution of the Ag, Ti, and O elements. Moreover, by studying the surface morphology of Ag@TiO_2, it was found that TiO_2 nanoparticles were successfully accumulated on the surface of Ag. Construction of plasmonic metal/semiconductor hybrid structures has been shown to be an advanced technique for enhancing photocatalytic activity [35].

The crystalline phases of Ag, TiO_2, and Ag@TiO_2 were determined by observing the X-diffraction peak positions in Fig. 4(a). Several diffraction peaks are observed at $2\theta = 25.3°$, 48.4°, 54.6°and 55.4°, which accord with (101), (200), (105), and (211) of anatase TiO_2, respectively. The characteristic diffraction peaks at diffraction angles of 38.2°, 44.4°, 64.6°, 77.5°and 81.6° correspond to the (111), (200), (220), (311), and (222) crystal surfaces, respectively. All diffraction peaks correspond to Ag (JCPDS File No: 87-0597). The purple line corresponds to the XRD spectrum of Ag@TiO_2 prepared by magnetron sputtering. The diffraction peaks of both Ag and TiO_2 can be identified and the phase structure of the prepared Ag@TiO_2 was pure anatase TiO_2. Moreover, Fig. 4(b) shows the Raman spectrum of the Ag@TiO_2 composite, which further characterizes the structure of the material. Five vibrational modes can be observed at 145.3, 199.2, 395.5, 515.3, and 639.8 cm^{-1}, corresponding to the $Eg_{(1)}$, A_{1g}, B_{1g}, $A_{1g} + B_{1g}$, and $Eg_{(2)}$ Raman active modes of anatase TiO_2, respectively. The elemental binding energy and specific surface composition of Ag@TiO_2 can be analyzed by X-ray

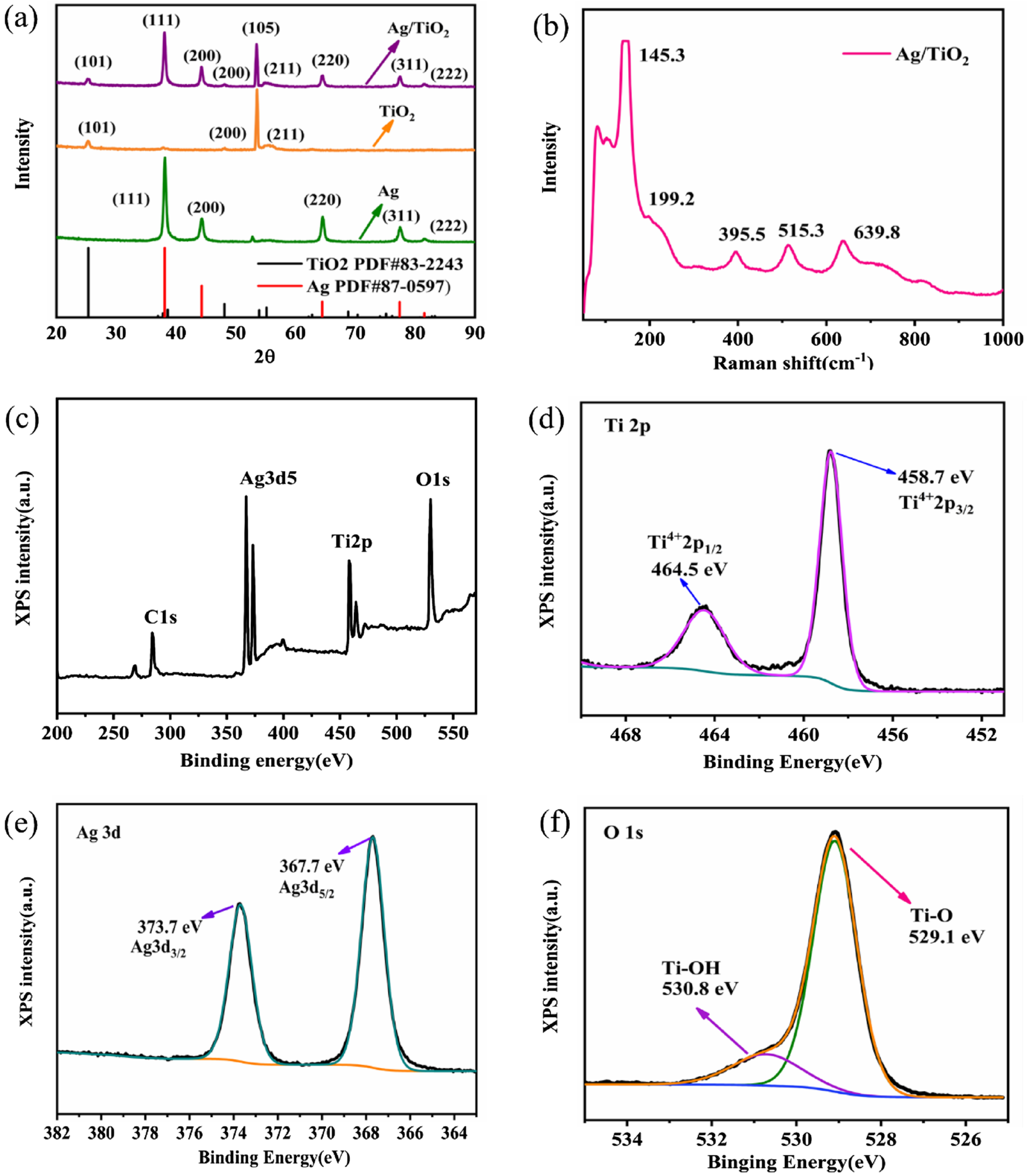

Figure 4: (a) XRD diffractograms of Ag, TiO$_2$, Ag/TiO$_2$. (b) Raman spectrum of Ag/TiO$_2$. (c) XPS full spectrum of Ag@TiO$_2$ composite; (d) XPS spectrum of Ti 2p; (e) XPS spectrum of Ag 3d; (f) XPS spectrum of O$_{1s}$.

photoelectron spectroscopy (XPS). It can further explore the interaction of Ag with TiO$_2$. By analyzing the XPS full spectrum [Fig. 4(c)], it was found that Ag, Ti, O, and C elements were present in the sample. Impurities and residual organic molecules contribute to the presence of C. Figure 4(d) shows the Ti (2p$_{1/2}$) and Ti (2p$_{3/2}$) peaks of the Ag@TiO$_2$ sample at binding energies of ≈ 464.4 and ≈ 458.7 eV, respectively. The gap between Ti (2p$_{1/2}$) and Ti (2p$_{3/2}$) core levels is 5.7 eV, which further clarifies that the titanium in the as-prepared Ag@TiO$_2$ is mainly Ti^{4+}. Furthermore, to illustrate the presence of Ag, the Ag 3d spectra of Ag@TiO_2 are given in Fig. 4(e). Two peaks appear at 373.7 and 367.7 eV, corresponding to the binding energies of Ag $3d_{3/2}$ and Ag $3d_{5/2}$, respectively. The difference between them is 6.0 eV, which is a typical characteristic of metallic Ag [36, 37]. In Fig. 4(f), all O_{1s} spectra show two peaks at 530.8 and 529.1 eV, the former is caused by oxygen vacancy and the latter is attributed to the lattice oxygen of TiO_2 (Ti–O).

Catalytic graphitization of PAN by Ag@TiO_2 composites

In this section, we explore the catalytic graphitization performance of Ag@TiO_2 polyacrylonitrile. The Ag@TiO_2 photocatalyst was subjected to an in situ photocatalytic reaction under a light source with a Raman spectrum at a wavelength of 532 nm. Firstly, as shown in Fig. 5(a), we can clearly see that the structure of the polyacrylonitrile molecule coated on the silicon wafer has not changed and still maintains its original powder-like molecular structure. 1470 cm^{-1} (δ-CH), 2240 cm^{-1} (υ-C≡N), and 2930 cm^{-1} (υ-CH2) are the wavenumber positions of the Raman peaks of PAN molecules, respectively. In addition, when the light source of the Raman spectrum interacts with the polyacrylonitrile on the Ag surface, the structure of the polyacrylonitrile changes, and the characteristic peaks after the graphitization of PAN appear in the Raman spectrum, at 1360 cm^{-1}, 1590 cm^{-1}, and 2700 cm^{-1} correspond to the D peak, G peak, and 2D peak after graphitization, respectively. This point can explain that the high energy generated by the interaction of metallic Ag with light drives the catalytic graphitization of PAN on the Ag surface. This reason can be attributed to the SPR effect of the interaction between metallic Ag and light [38]. The SPR effect will generate a large number of carriers in the non-radiative decay process, which can change the structure of PAN and be graphitized.

In general, the relative intensity ratio of the D peak to the G peak is usually used to characterize the defect density of graphite or graphene [39], that is to say, the degree of graphitization of polyacrylonitrile or the defects present in it is related to the intensity ratio (I_D/ I_G), the higher the degree of graphitization, the smaller the I_D/I_G ratio. It can be seen from Fig. 5(a, b) that the graphitization degree of PAN on the Ag@TiO_2 nanostructure surface is higher after the interaction with light, and the ratio of the relative intensity of the D peak to the G peak (I_D/I_G) is lower. On the one hand, Ag has superior plasmonic properties compared to Cu. We can observe the catalytic properties of Cu and Ag in Fig. S2, and the activation energy provided by the hot electrons induced by plasma catalysis can drive the increase in the degree of graphitization of PAN [6]; on the other hand, the construction of a plasmonic metal Ag and TiO_2 semiconductor hybrid structure can expand the optical responsive region and improve the separation efficiency of hot electron–hole pairs in photocatalysis [40]. Compared with Ag alone to improve the catalytic graphitization of PAN, the Ag@TiO_2 nanostructured composite has more superior performance for the PAN-catalyzed graphitization. Therefore, the low-temperature catalytic graphitization of polyacrylonitrile is enhanced by introducing Ag@TiO_2 nanostructures as plasmonic photocatalysts. Therefore, we are able to demonstrate that the graphitization of PAN has been significantly increased in the presence of Ag@TiO_2 photocatalytic systems as compared to pure TiO_2 and Ag nanocrystals.

However, the evaporation temperature of the removed solvent is also an important influence on the catalytic graphitization of polyacrylonitrile. As shown in Fig. 6, the intensity of graphite D peak increases with the increase of temperature, and the increase of D peak intensity indicates the existence of a large number of defects [41]. It can be seen from Table 1 that the ratio of the relative intensities of the D peak to the G peak (I_D/I_G) increases with the increase of temperature, and high temperature conditions will affect the catalytic graphitization

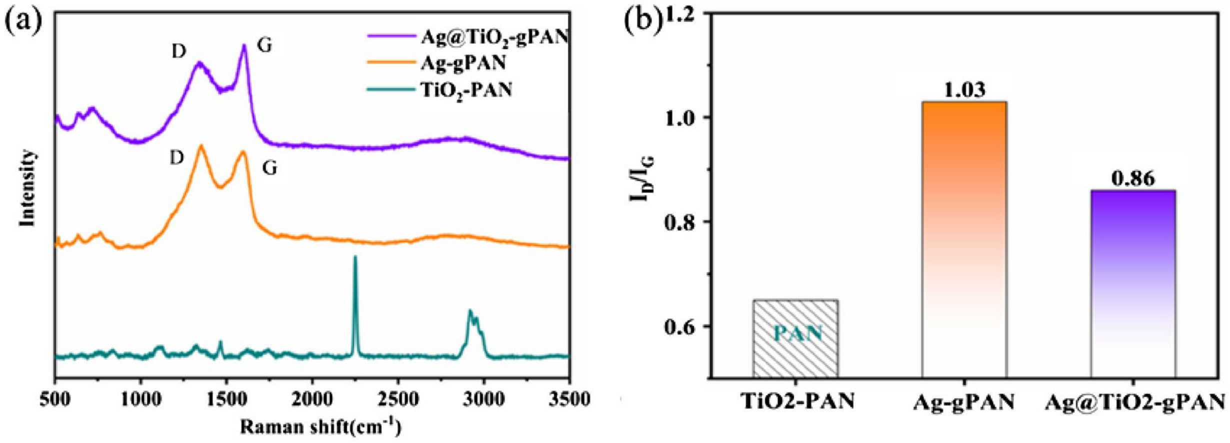

Figure 5: (a) In situ Raman spectra of PAN on Si, Ag, and Ag@TiO_2 surfaces (80 °C); (b) I_D/I_G ratios of graphitized PAN on different substrates (80 °C).

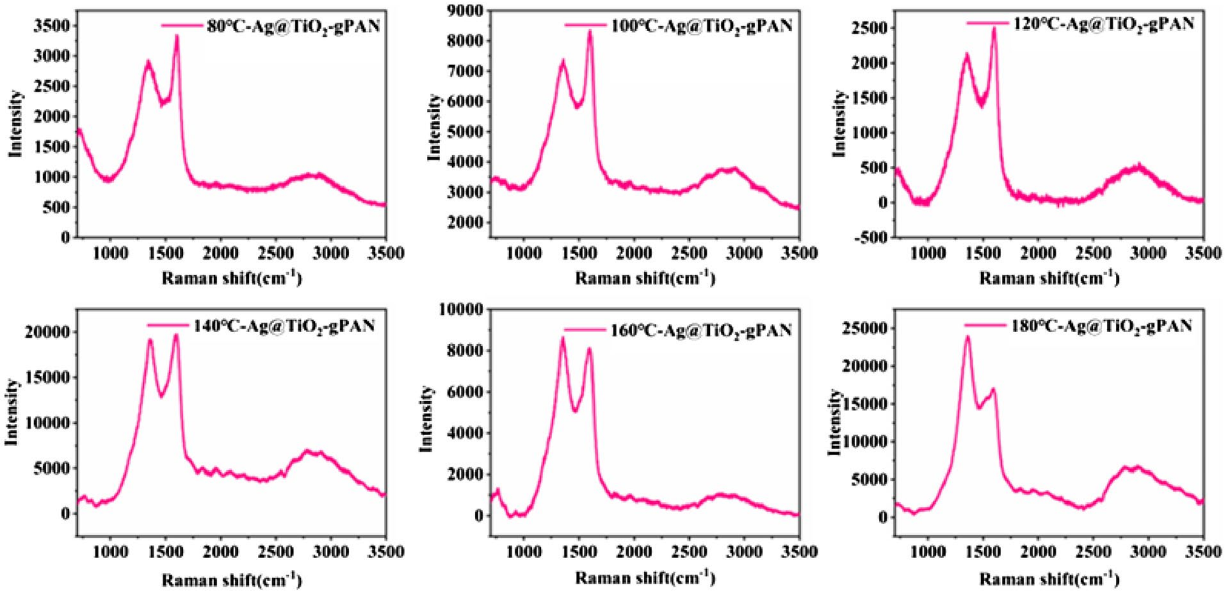

Figure 6: The volatilization temperature of the solvent also affects the catalyzed graphitization of polyacrylonitrile.

TABLE 1: Ratio of the relative intensities of the D and G peaks of polyacrylonitrile-catalyzed graphitization.

temperature(°C)	80 °C	100 °C	120 °C	140 °C	160 °C	180 °C
D (cm^{-1})	1350	1358	1362	1357	1358	1366
G (cm^{-1})	1601	1598	1600	1599	1600	1589
I_D/I_G	0.87	0.88	0.85	0.97	1.08	1.43

performance of nanostructures on PAN. This is mainly attributed to the fact that Ag nanostructures are easily oxidized at high temperatures and a layer of Ag_2O is formed on the surface of Ag nanoparticles. Therefore, the interaction between light and Ag_2O can only produce a weak SPR effect, which leads to a reduction in the photocatalytic activity of Ag@TiO_2 [42]. Below 80 °C, the solvent dimethylformamide (DMF) of PAN is not completely volatilized due to the lower temperature. The presence of DMF hinders the graphitization of PAN, which is shown in Figs. S3 and S4.

Ag@TiO_2-catalyzed graphitization mechanism of PAN

The performance of photocatalysis is affected by the photoresponse. Figure 7(a) shows the UV–vis diffuse reflectance spectrum (DRS) of the obtained samples. We investigated the optical properties of the samples by analyzing their DRS. It can be seen that the pristine TiO_2 shows strong absorption in the UV region and the absorption edge located at 380 nm, which is consistent with the light absorption properties of anatase TiO_2. In addition, it can be seen that the Ag nanoparticles have an absorption peak at 320 nm, which is attributed to the SPR of the Ag nanoparticles. Interestingly, upon loading TiO_2 nanocrystals, as for Ag@TiO_2, an obvious peak at 400–650 nm appeared, its response to visible light is significantly enhanced.

This phenomenon can be attributed to the following two principal reasons. On the one hand, Ag nanoparticles have a well-known SPR effect, which significantly boosts the absorption of visible light [43]. On the other hand, Schottky barriers are created at the interface of the plasmonic metal/semiconductor hybrid structure [44]. The Schottky barriers will lead to the transfer of hot electrons generated by plasmonic metal Ag to the conduction band of porous TiO_2, which can effectively improve the separation efficiency of hot electron–hole pairs in photocatalysis [45]. Photoluminescence (PL) spectroscopy can be used to evaluate the charge separation ability. We all know that photoexcited electrons and holes undergo several processes for recombination, and the efficiency of their recombination can be reflected by the PL spectral intensity. Figure 7(b) shows the photoluminescence (PL) spectra of above three photocatalysts. The PL intensity for Ag@TiO_2 was much lower than that of Ag, TiO_2, this result indicates that the formation of Schottky junctions between TiO_2 and Ag nanocrystals reduces the recombination of charge carriers, resulting in a longer-lived carriers (electron/hole pair) [46].

Meanwhile, the transient photocurrent response can also predict the photocatalytic activity. The transient photocurrent

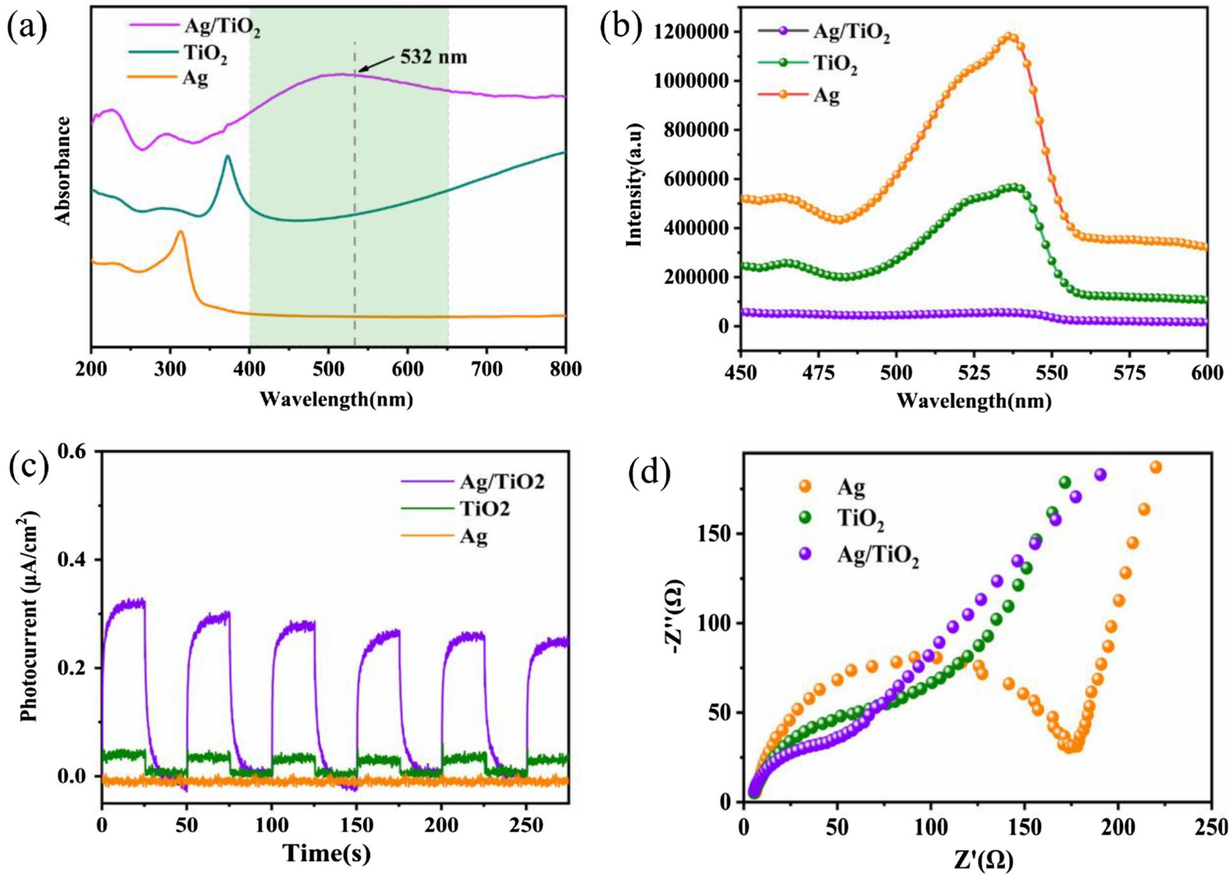

Figure 7: (a) UV–vis spectra of Ag, TiO_2, Ag/TiO_2; (b) The PL spectra of Ag, TiO_2, Ag/TiO_2; (c) Photocurrent responses in the light on–off process; (d) shows the electrochemical impedance results of the Ag, TiO_2, Ag/TiO_2.

responses of Ag, TiO_2, Ag@TiO_2 are displayed in Fig. 7(c), the photocurrent of the Ag nanoparticles is very weak which is negligible. Notably, the photocurrent density of the Ag@TiO_2 structure reaches 0.33 $\mu A/cm^{-2}$, which is nearly 10 times higher than that of traditional TiO_2 (0.034 mA/cm^{-2}). This further illustrates that the special structure of the Ag@TiO_2 composite and its enhanced SPR intensity contribute to the enhanced photoresponse ability. Electrochemical impedance spectroscopy (EIS) can be used to explore the interface properties between electrodes and electrolytes. In Fig. 7(d), the diameter of the semicircle represented the charge transfer resistance, and the semicircle in the high frequency Nyquist plot reflected the charge transfer process. We found that the arch for Ag@TiO_2 is much smaller than TiO_2 and Ag under visible light (> 420 nm) illumination, which indicates that the modification of Ag can significantly improve the electron mobility by reducing the recombination of electron–hole pairs. Through the comparative analysis of different sample, the arch value for TiO_2 was in the middle among them. Taken together, these results implicated that Ag@TiO_2 nanostructures can expand the response region of light and the Ag nanocrystals be able to possess strong SPR effect.

We simulated the near-field distributions of the Ag@TiO_2 nanostructures by means of the finite difference time domain (FDTD) method, which is beneficial to study the catalytic graphitization of PAN by SPR effect. As shown in Fig. 8(a), a single Ag@TiO_2 local electric field distribution model was simulated, it can be seen that the TiO_2 nanoparticles are loaded on the surface of the relatively large Ag nanoparticles. Figure 8(b) illustrate the electric field distributions of the Ag@TiO_2 corresponding to the 532 nm wavelength. Additionally, Fig. 8(c) shows high local electric field distribution of the dotted portion in Fig. 8(b). The FDTD simulations show that the highest plasmonic electric field intensities are generated between the TiO_2 and the spherical Ag nanoparticles. These spots with an enhanced electric field are referred to as "hot spots". Not surprisingly, it is found that there exists strong localized electric field between two nanoparticles, and the intensity of the electric field at the space between two nanoparticles is approximately 3 times stronger than that of a single nanoparticle, as shown in Fig. 8(e, f). Higher electromagnetic field generates more hot electron, which provide activation energy and can exhibit significant catalytic effects on the surface of Ag@TiO_2

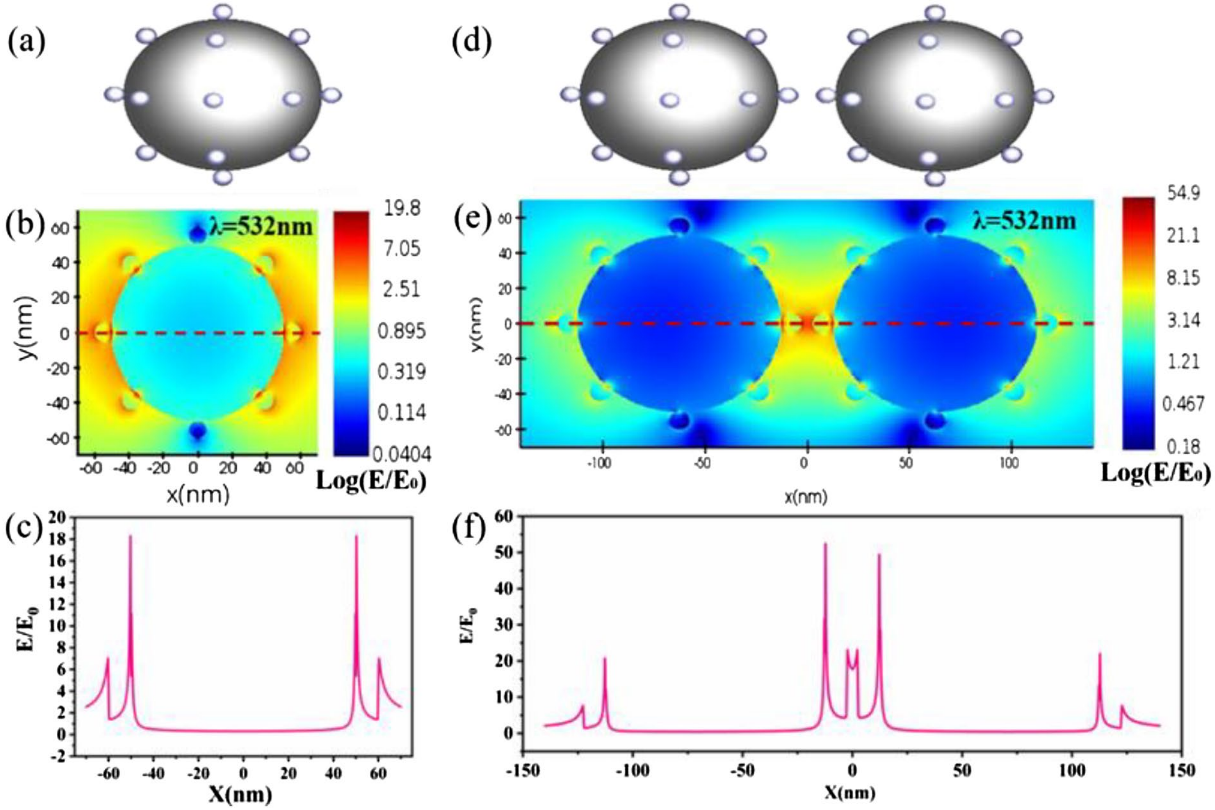

Figure 8: FDTD simulation of the electric field distribution of Ag/TiO_2. (a) model of a single Ag@TiO_2 nanoparticle; (b) local field strength of a single Ag@TiO_2 nanoparticle; (c) local field strength corresponding to the red dashed line in (b) for a single Ag@TiO_2 nanoparticle; (d) model of two Ag@TiO_2 nanoparticles; (e) local field strength of two Ag@TiO_2 nanoparticles; (f) local field strength corresponding in (e) field strengths.

nanostructures. This effect is nicely captured by the following equation, where the rate of plasmon-induced hot carrier generation can be estimated [47].

$$P_{MFP} = \frac{1}{2}\int_{V_{MFP}} dr|E(r)|^2 \mathrm{Im}(\varepsilon),$$

where P_{MFP} is the optical absorption within the mean free path length of the transmission interface, V_{MFP} is the under consideration metallic volume that includes the mean free path of the transmission interface, and the local electric field intensity is represented by $|E(r)|^2$. Im(ε) is the imaginary part of the material's dielectric function. We can find that the excitation rate of hot carriers due to the implementation of SPR effect on plasmonic nanostructures is greatly affected by the local electric field distribution. Meanwhile, the high electromagnetic field of LSPR and strong coupling between Ag nanoparticles(NPs) and TiO_2 will benefit the plasmon-induced charge transportation and separation, which can promote the chemical transformation procedures [48]. More importantly, the FDTD simulations confirm our experimental findings. The improved graphitization of polyacrylonitrile is attributed to the SPR effect of Ag in Ag@TiO_2 nanostructures and improves charge separation transport.

So far, we show the catalytic mechanism of PAN-catalyzed graphitization in terms of both experiments and theoretical simulation in detail. Figure 9 shows the mechanism of SPR-enhanced the catalytic graphitization of PAN on the surface of the periodic Ag@TiO_2 nanocomposite under 532 nm irradiation. On the one hand, by analyzing the UV–vis-NIR absorption spectra of Ag@TiO_2 and TiO_2, it is found that the SPR effect of Ag can lead to the enhanced absorption of Ag@TiO_2 in the entire spectral range. [49]. Besides, the generation of charge carriers in the Ag follows excitation and decay of surface plasmons, generating both electrons and holes with excess energy, following transferring to PAN molecules to trigger chemical reaction. Moreover, due to the Schottky contact between Ag and TiO_2, a built-in electric field is generated to promote the separation of photogenerated electrons and holes and increase the lifetimes of carriers. This implies that more charge carriers will be involved in the catalytic reaction. The results of this study can be verified by measurements of PL spectra and transient photocurrent responses. The photocatalytic enhancement observed under light illumination can be understood by simulating the electromagnetic response of the Ag@TiO_2 photocatalysts using the FDTD method. Simulation results clearly confirm the presence of localized SPR-enhanced electromagnetic field for the Ag and

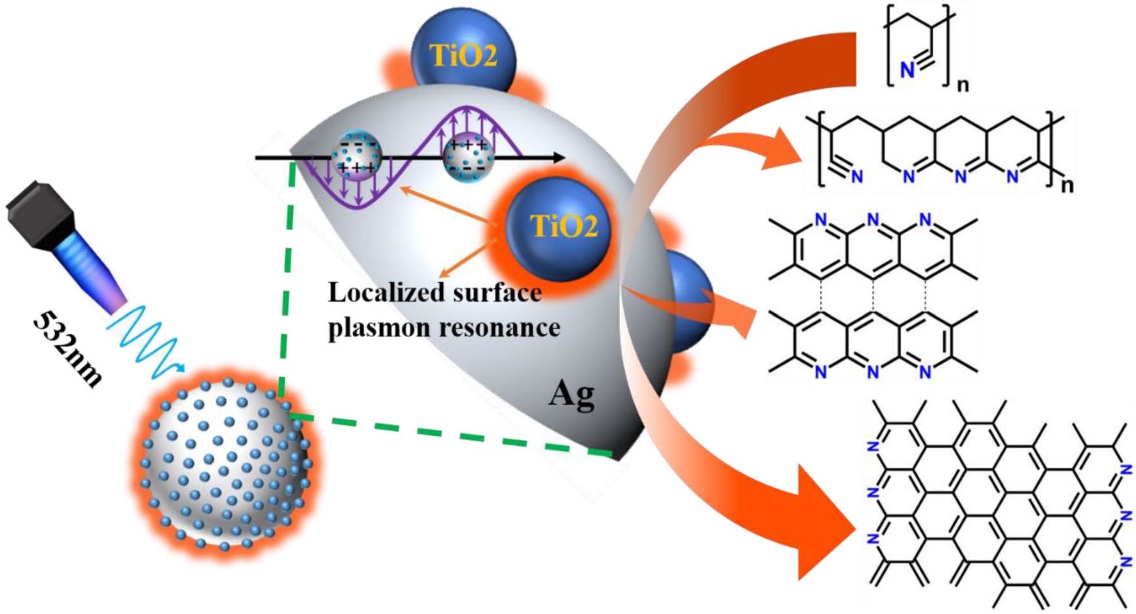

Figure 9: Mechanisms of polyacrylonitrile-catalyzed graphitization on Ag@TiO_2 surfaces.

TiO_2. The enhanced electromagnetic field improves the light absorption of TiO_2 and benefit the plasmon-induced charge transportation and separation. Since the rate of hot electron generation is proportional to the intensity of the local electric field, more carriers are involved in the chemical reaction during photocatalysis. It means that the catalytic graphitization of polyacrylonitrile is further enhanced.

Conclusion

In this work, we have successfully prepared Ag@TiO_2 photocatalysts with the plasmonic properties by applying magnetron sputtering, which have high catalytic activity for enhancing the catalytic graphitization of PAN. Experimental results indicated that the SPR effect of Ag nanostructures is a critical element driving the graphitization of PAN, expanding the response region of light and improving the separation efficiency of hot electron–hole pairs, which can be achieved by constructing plasmonic metal (Ag)/semiconductor (TiO_2) hybrid structures. As depicted by 3D FDTD simulations, in the case of densely dispersed TiO_2 nanoparticles on Ag, enhancing greatly local electric field near the surface of the nanostructures and result in strong optical response. Consequently, Ag@TiO_2 nanostructures exhibit high catalytic activity for enhancing the catalytic graphitization of PAN under 532 nm light illumination in comparison with the bare Ag. The experimental results are consistent with theoretical simulations. This research work further promotes the application of plasmonic photocatalysts in catalytic reactions, energy, and environment.

Experimental section

Preparation of Ag@TiO_2

Magnetron sputtering (MS) is a well-known physical vapor deposition process that is used to synthesize nanoparticles or thin films. Ag@TiO_2 composite material is effectively prepared by magnetron sputtering method. Ti and Ag targets were sonicated with acetone, deionized water, and ethanol for 30 min, respectively. Then, Ti and Ag targets were pre-sputtered for 10 min to remove impurities from the surface. The pressure of the sputtering chamber was adjusted to below 2.0×10^{-5} Pa, and TiO_2 was prepared by sputtering the Ti target in a mixed atmosphere of O_2 and Ar (3/7 in volume ratio) at 125W. The sputtering time was 120 min. Finally, Ag was deposited in TiO_2 under vacuum. The sputtering time was also 120 min.

Material characterization

Scanning electron microscopy(SEM) studies were carried out on Nova Nano SEM 450 for the morphological characterization. The crystal structures were characterized by an X-Ray diffractometer (Panalytical Xpert3 Powder) using Cu Kα radiation source ($\lambda = 0.15406$ nm). The Raman spectra was carried out using a laser confocal Raman micro-spectroscopy (LabRAM HR800, Horiba JobinYvo) with excitation at 532 nm and 50mW. The binding energy and chemical state of the Ag surface was identified by the XPS (Ultra-DLD Kratos Axis) instrument. UV–vis diffuse reflectance spectroscopy (UV–vis DRS) was obtained with a Perkin-Elmer spectrophotometer, which can evaluate the optical properties of nanocomposites. The photoluminescence (PL) spectra of the photocatalysts were obtained by an F7000 (Hitachi, Japan) photoluminescence detector with an excitation wavelength of 325 nm. Photoelectrochemical measurements were carried out in a conventional three electrode setup on an electrochemical station, and the light source is a xenon lamp with a broadband Visible to NIR spectrum. A 0.1 M Na_2 SO_4 aqueous solution was used as the electrolyte. To study the optical properties of the Ag@TiO_2 composite structure, we performed electrodynamic simulations using the FDTD method. According to the SEM and EDS images shown in Fig. 3, the spherical Ag nanoparticles were approximately 100 nm in size and smaller sized TiO_2 particles were loaded on Ag surface. By consulting the literature, we obtained the relevant data of the frequency-dependent complex dielectric constants of Ag and TiO_2. The frequency-dependent complex dielectric constants of Ag and TiO_2 is shown are in Fig. S1.

Acknowledgements

This work was supported by the National Natural Science Foundation of China (51662023, 11674136, 61901200) and the Yunnan Fundamental Research Projects (2019FD041, 202101AW070010).

Data availability

The data that support the findings of this study are available from the corresponding author, [H.L. Tan], upon reasonable request.

Declarations

Conflict of interest The authors declare that they have no known competing financial interests or personal relationships that could have appeared to influence the work reported in this paper.

Supplementary Information

The online version contains supplementary material available at https://doi.org/10.1557/s43578-023-00931-z.

References

1. Y. Zhao, W. Gao, S. Li, G.R. Williams, A.H. Mahadi, D. Ma, Solar-versus thermal-driven catalysis for energy conversion. Joule **3**, 920–937 (2019)
2. G. Knör, Photocatalytic reactions of porphyrin-based multielectron transfer sensitizers. Coord. Chem. Rev. **171**, 61–70 (1998)
3. J.A. Rodríguez, J. Hrbek, Inverse oxide/metal catalysts: a versatile approach for activity tests and mechanistic studies. Surf. Sci. **604**, 241–244 (2010)
4. R. Jiang, F. Qin, Y. Liu, X.Y. Ling, J. Guo, M. Tang, S. Cheng, J. Wang, Gold nanocups: colloidal gold nanocups with orientation-dependent plasmonic properties (Adv. Mater. 30/2016). Adv. Mater. **28**, 6266–6266 (2016)
5. J. Peral, D. Ollis, Heterogeneous photocatalytic oxidation of gas-phase organics for air purification: acetone, 1-butanol, butyraldehyde, formaldehyde, and m-xylene oxidation. J. Catal. **136**, 554–565 (1992)
6. Z. Zhang, J. Lu, X. Ren, N. Sun, J. Liu, Y. Zhou, Y. Gao, J. Cai, X. Cai, H. Tan, Enhancement of the low-temperature catalytic graphitization of polyacrylonitrile by incorporating Cu nanostructures as plasmonic photocatalyst. J. Mater. Sci. **57**, 1703–1713 (2022)
7. S. Che, C. Li, C. Wang, W. Zaheer, X. Ji, B. Phillips, G. Gurbandurdyyev, J. Glynn, Z.H. Guo, M. Al-Hashimi, H.C. Zhou, S. Banerjee, L. Fang, Solution-processable porous graphitic carbon from bottom-up synthesis and low-temperature graphitization. Chem. Sci. **12**, 8438–8444 (2021)
8. H. Chen, J. Yang, Q. Shuai, J. Li, Q. Ouyang, S. Zhang, In-situ doping B4C nanoparticles in PAN precursors for preparing high modulus PAN-based carbon fibers with boron catalytic graphitization. Compos. Sci. Technol. **200**, 108455 (2020)
9. D. He, F. Zhang, S. Xu, W. Yu, Q. Cai, T.J. LaTempa, C.A. Grimes, Synergistic catalytic effect of Ti–B on the graphitization of polyacrylonitrile-based carbon fibers. Carbon **46**, 1506–1508 (2008)
10. S. Yi, Z. Fan, C. Wu, J. Chen, Catalytic graphitization of furan resin carbon by yttrium. Carbon **46**, 378–380 (2008)
11. R. Wang, G. Lu, H. Zhuang, J. Yu, Synergistic catalytic effect of light rare earth element and other additives on the degree of graphitization and properties of graphite. J. Mater. Sci. **52**, 663–673 (2016)
12. X. Xiu, L. Hou, J. Yu, S. Jiang, L. Chonghui, X. Zhao, P. Qianqian, S. Qiu, C. Zhang, B. Man, Z. Li, Manipulating the surface-enhanced Raman spectroscopy (SERS) activity and plasmon-driven catalytic efficiency by the control of Ag NP/graphene layers under optical excitation. Nanophotonics **10**, 20200644 (2021)
13. Z. Zhang, M. Sun, P. Ruan, H. Zheng, H. Xu, Electric field gradient quadrupole Raman modes observed in plasmon-driven catalytic reactions revealed by HV-TERS. Nanoscale **5**, 4151–4155 (2013)
14. P. Zhang, G. Zeng, T. Song, S. Huang, T. Wang, H. Zeng, Design of plasmonic CuCo bimetal as a nonsemiconductor photocatalyst for synchronized hydrogen evolution and storage. Appl. Catal. B **242**, 389–396 (2019)
15. Y. Qin, Y. Guo, Z. Liang, Y. Xue, X. Zhang, L. Yang, J. Tian, Au nanorods decorated TiO_2 nanobelts with enhanced full solar spectrum photocatalytic antibacterial activity and the sterilization file cabinet application. Chin. Chem. Lett. **32**, 1523–1526 (2021)

16. B. Fang, Z. Xing, D. Sun, Z. Li, W. Zhou, Hollow semiconductor photocatalysts for solar energy conversion. Adv. Powder Mater. **1**, 100021 (2022)
17. X. Qian, Y. Wei, M. Sun, Y. Han, X. Zhang, J. Tian, M. Shao, Heterostructuring 2D TiO_2 nanosheets in situ grown on Ti_3C_2Tx MXene to improve the electrocatalytic nitrogen reduction. Chin. J. Catal. **43**, 1937–1944 (2022)
18. V. Kumar, S.C. O'Donnell, D.L. Sang, P.A. Maggard, G. Wang, Harnessing plasmon-induced hot carriers at the interfaces with ferroelectrics. Front. Chem. (2019). https://doi.org/10.3389/fchem.2019.00299
19. B. Zeng, S. Wang, Z. Feng, Y. Xiao, M. Li, F. Hong, Y. Zhao, Z. Feng, R. Li, C. Li, Atomically unraveling the dependence of surface microstructure on plasmon-induced hydrogen evolution on $Au/SrTiO_3$. Nano Energy **91**, 106638 (2022)
20. C. Zhang, F. Jia, Z. Li, X. Huang, G. Lu, Plasmon-generated hot holes for chemical reactions. Nano Res. **13**, 3183–3197 (2020)
21. Y. Zhang, W. Zhou, Y. Tang, Y. Guo, Z. Geng, L. Liu, X. Tan, H. Wang, T. Yu, J. Ye, Unravelling unsaturated edge S in amorphous NiSx for boosting photocatalytic H2 evolution of metastable phase CdS confined inside hydrophilic beads. Appl. Catal. B **305**, 121055 (2022)
22. S. Li, M. Cai, Y. Liu, C. Wang, R. Yan, X. Chen, Constructing $Cd_{0.5}Zn_{0.5}S/Bi_2WO_6$ S-scheme heterojunction for boosted photocatalytic antibiotic oxidation and Cr(VI) reduction. Adv. Powder Mater. **2**, 100073 (2023)
23. S. Li, M. Cai, Y. Liu, C. Wang, K. Lv, X. Chen, S-Scheme photocatalyst $TaON/Bi_2WO_6$ nanofibers with oxygen vacancies for efficient abatement of antibiotics and Cr(VI): Intermediate eco-toxicity analysis and mechanistic insights. Chin. J. Catal. **43**, 2652–2664 (2022)
24. S. Li, M. Cai, Y. Liu, J. Zhang, C. Wang, S. Zang, Y. Li, P. Zhang, X. Li, In situ construction of a $C3N5$ nanosheet/Bi_2WO_6 nanodot S-scheme heterojunction with enhanced structural defects for the efficient photocatalytic removal of tetracycline and Cr(vi). Inorg. Chem. Front. **9**, 2479–2497 (2022)
25. C. Wang, R. Yan, M. Cai, Y. Liu, S. Li, A novel organic/inorganic S-scheme heterostructure of TCPP/Bi12O17Cl2 for boosting photodegradation of tetracycline hydrochloride: kinetic, degradation mechanism, and toxic assessment. Appl. Surf. Sci. **610**, 155346 (2023)
26. M. Cai, C. Wang, Y. Liu, R. Yan, S. Li, Boosted photocatalytic antibiotic degradation performance of $Cd_{0.5}Zn_{0.5}S$/carbon dots/Bi_2WO_6 S-scheme heterojunction with carbon dots as the electron bridge. Sep. Purif. Technol. **300**, 121892 (2022)
27. S. Li, C. Wang, M. Cai, Y. Liu, K. Dong, J. Zhang, Designing oxygen vacancy mediated bismuth molybdate (Bi_2MoO_6)/N-rich carbon nitride (C3N5) S-scheme heterojunctions for boosted photocatalytic removal of tetracycline antibiotic and Cr(VI): intermediate toxicity and mechanism insight. J. Colloid Interface Sci. **624**, 219–232 (2022)
28. Y. Zhang, J. Zhao, H. Wang, B. Xiao, W. Zhang, X. Zhao, T. Lv, M. Thangamuthu, J. Zhang, Y. Guo, J. Ma, L. Lin, J. Tang, R. Huang, Q. Liu, Single-atom Cu anchored catalysts for photocatalytic renewable H2 production with a quantum efficiency of 56%. Nat. Commun. **13**, 58 (2022)
29. Z. Yin, Y. Wang, C. Song, L. Zheng, N. Ma, X. Liu, S. Li, L. Lin, M. Li, Y. Xu, W. Li, G. Hu, Z. Fang, D. Ma, Hybrid Au–ag nanostructures for enhanced Plasmon-driven catalytic selective hydrogenation through visible light irradiation and surface-enhanced Raman scattering. J. Am. Chem. Soc. **140**, 864–867 (2018)
30. H. Tong, S. Ouyang, Y. Bi, N. Umezawa, M. Oshikiri, J. Ye, ChemInform abstract: nano-photocatalytic materials: possibilities and challenges. Adv. Mater. (Deerfield Beach, Fla.) **24**, 229–51 (2012)
31. C. Hou, H. Liu, M.F. Bakhtari, Preparation of Ag SPR-promoted TiO_2-{001}/$HTiOF_3$ photocatalyst with oxygen vacancies for highly efficient degradation of tetracycline hydrochloride. Mater. Sci. Semicond. Process. **136**, 106142 (2021)
32. X. Ma, Z. Cheng, M. Tian, X. Liu, X. Cui, Y. Huang, S. Tan, J. Yang, B. Wang, Formation of plasmonic polarons in highly electron-doped anatase TiO_2. Nano Lett. **21**, 430–436 (2021)
33. W. Deng, K. Dayongjin, J. Drozdowicz-Tomsia, J. Yuan, E.M. Wu, Ultrabright Eu-doped plasmonic $Ag@SiO_2$ nanostructures: time-gated bioprobes with single particle sensitivity and negligible background. Adv. Mater. **23**, 4649–4654 (2011)
34. J. Yoo, X. Ma, W. Tang, G.-C. Yi, Metal-lined semiconductor nanotubes for surface Plasmon-mediated luminescence enhancement. Nano Lett. **13**, 2134–2140 (2013)
35. D. Venieri, A. Fraggedaki, M. Kostadima, E. Chatzisymeon, V. Binas, A. Zachopoulos, G. Kiriakidis, D. Mantzavinos, Solar light and metal-doped TiO_2 to eliminate water-transmitted bacterial pathogens: photocatalyst characterization and disinfection performance. Appl. Catal. B **154–155**, 93–101 (2014)
36. X. Shi, Y. Ding, S. Zhou, B. Zhang, M. Cai, J. Yao, L. Hu, J. Wu, S. Dai, M.K. Nazeeruddin, Enhanced interfacial binding and electron extraction using boron-doped TiO_2 for highly efficient hysteresis-free perovskite solar cells. Adv. Sci. (Weinh) **6**, 1901213 (2019)
37. M. Xu, Y. Wang, J. Geng, D. Jing, Photodecomposition of NOx on Ag/TiO_2 composite catalysts in a gas phase reactor. Chem. Eng. J. **307**, 181–188 (2017)
38. G. Tian, Y. Chen, W. Zhou, K. Pan, Y. Dong, C. Tian, H. Fu, Facile solvothermal synthesis of hierarchical flower-like Bi_2MoO_6 hollow spheres as high performance visible-light driven photocatalysts. J. Mater. Chem. **21**, 887–892 (2011)
39. T. Schranghamer, A. Oberoi, Graphene memristive synapses for high precision neuromorphic computing. Nat. Commun. (2020). https://doi.org/10.1038/s41467-020-19203-z
40. N. Sun, Y. Zhang, X. Li, Y. Jing, Z. Zhang, Y. Gao, J. Liu, H. Tan, X. Cai, J. Cai, Ultrathin g-PAN/PANI-encapsulated Cu

nanoparticles decorated on $SrTiO_3$ with high stability as an efficient photocatalyst for the H2 evolution and degradation of 4-nitrophenol under visible-light irradiation. Catal. Sci. Technol. **12**, 2482–2489 (2022)

41. J. Cai, P. Ruffieux, R. Jaafar, M. Bieri, T. Braun, S. Blankenburg, M. Muoth, A.P. Seitsonen, M. Saleh, X. Feng, K. Müllen, R. Fasel, Atomically precise bottom-up fabrication of graphene nanoribbons. Nature **466**, 470–473 (2010)
42. F. Tong, Z. Lou, X. Liang, F. Ma, W. Chen, Z. Wang, Y. Liu, P. Wang, H. Cheng, Y. Dai, Z. Zheng, B. Huang, Plasmon-induced dehydrogenation of formic acid on Pd-dotted Ag@Au hexagonal nanoplates and single-particle study. Appl. Catal. B **277**, 119226 (2020)
43. Z. Xiong, F. Qin, P.-S. Huang, I. Nettleship, J.-K. Lee, Effect of synthesis techniques on crystallization and optical properties of Ag-Cu bimetallic nanoparticles. JOM **68**, 1163 (2016)
44. S.-U. Lee, H. Jung, D.H. Wi, J.W. Hong, J. Sung, S.-I. Choi, S.W. Han, Metal–semiconductor yolk–shell heteronanostructures for plasmon-enhanced photocatalytic hydrogen evolution. J. Mater. Chem. A **6**, 4068–4078 (2018)
45. J. Liu, J. Zheng, G. Yue, H. Li, Z. Liu, Y. Zhao, N. Wang, C. Sun, Z. Cui, Continuous g-C3N4 layer-coated porous TiO_2 fibers with enhanced photocatalytic activity toward H2 evolution and dye degradation. RSC Adv. **12**, 10258–10266 (2022)
46. D. Deng, K. Novoselov, Q. Fu, N. Zheng, Z.-Q. Tian, X. Bao, ChemInform abstract: catalysis with two-dimensional materials and their heterostructures. ChemInform (2016). https://doi.org/10.1002/chin.201623245
47. P. Christopher, M. Moskovits, Hot charge carrier transmission from plasmonic nanostructures. Annu. Rev. Phys. Chem. **68**, 379–398 (2017)
48. D. Chen, Q. Chen, L. Ge, L. Yin, B. Fan, H. Wang, H. Lu, H. Xu, R. Zhang, G. Shao, Synthesis and Ag-loading-density-dependent photocatalytic activity of Ag@TiO_2 hybrid nanocrystals. Appl. Surf. Sci. **284**, 921–929 (2013)
49. Z. Wang, J. Liu, W. Chen, Plasmonic Ag/AgBr nanohybrid: synergistic effect of SPR with photographic sensitivity for enhanced photocatalytic activity and stability. Dalton Trans. **41**, 4866–4870 (2012)